Mechanism and Reactivity Parameters of the Reduction of Arylmethyl Radicals from Time-Resolved Electron-Photoinjection Experiments

José Gonzalez, Philippe Hapiot, Valery Konovalov,[1] and Jean-Michel Savéant*

Contribution from the Laboratoire d'Electrochimie Moléculaire de l'Université Denis Diderot, Unité Mixte de Recherche Université—CNRS No 7591, 2 place Jussieu, 75251 Paris Cedex 05, France

Received May 26, 1998

Abstract: The 9-anthrylmethyl, diphenylmethyl, benzyl, and 4-methylbenzyl radicals are generated by reduction of the corresponding chlorides with electrons photoinjected in laser pulse experiments. The "polarograms" derived from the variation of the charge flowing through the electrode with the dc potential of the electrode represent the reduction of these radicals to the corresponding anions. The meaning of the half-wave potentials is investigated through their variations with the measurement time and with the addition of acids in the solution, which accelerates the disappearance of the carbanion. Correcting the kinetic data for the effect of radical dimerization, the reduction kinetics appear to be mostly under the control of the follow-up reaction of the carbanion with acids present in the medium, although the effect of charge-transfer kinetics begins to interfere at the lower end of the time window. The results are compared with earlier data obtained by other techniques. The changes in reactivity observed in the series are discussed with the help of density functional quantum chemical calculations.

The redox properties of free radicals are essential parameters for predicting whether electron transfer to molecules may trigger a radical or an ionic chemistry.[2] If these redox properties can be converted into standard potentials, they may then be used to estimate other thermodynamic parameters, such as pK_as and bond dissociation free energies.[3] Several direct or indirect electrochemical methods have been proposed for investigating the reduction characteristics of free radicals. However, none of them provides the reduction standard potential in a straightforward manner.

The simplest of these methods involves the recording of the oxidation wave of the anion in steady-state or cyclic voltammetry.[4] One drawback of this method is that it is limited to cases where the anion is sufficiently stable in the assay solution. The waves thus obtained are rarely reversible because of the instability of the radical (which often undergoes a rapid dimerization). Their half-wave or peak potentials, therefore, do not lead directly to the standard potential. Possibilities for circumventing this difficulty have been discussed.[5]

Direct reductive cyclic voltammetry may be used to investigate the reduction characteristics of transient free radicals, $R^{\bullet}$, generated in situ by reduction of a cleaving RX molecule,[2]

$$RX + e^{-}(\text{electrode}) \rightarrow R^{\bullet} + X^{-}$$
(in one step or in two steps)
$$R^{\bullet} + e^{-}(\text{electrode}) \rightleftharpoons R^{-}$$

The effects of second-order self-reactions of the radical (e.g., dimerization and H atom disproportionation) and of charge-transfer kinetics on the radical wave have been fully analyzed.[2,6] These treatments can be easily adapted to other reactions in which the radical and/or the anion would be engaged. One limitation of the method is that the leaving group, X, has to be selected so that the reduction potential of RX, at which the radical is generated, is less negative than the reduction potential of the radical.

An indirect electrochemical method, based on redox catalysis,[7] has also been applied to the determination of the reduction potential of transient radicals.[8] The reduced form, $Q^{\bullet -}$, of a reversible redox couple, $P/Q^{\bullet -}$ ($Q^{\bullet -}$ is usually an aromatic anion radical in a nonacidic solvent), serves as mediator of the electrochemical reduction of the radical generating substrate,

(1) Present address: Center for Materials for Information Technology, University of Alabama, P.O. Box 870209, Room 205 Bevill Building, Tuscaloosa, AL 35487.

(2) Andrieux, C. P.; Gallardo, I.; Savéant, J.-M. *J. Am. Chem. Soc.* **1989**, *111*, 1620.

(3) (a) Bordwell, F. G.; Zhang, X.-M. *Acc. Chem. Res*. **1993**, *26*, 510. (b) Wayner, D. M.; Parker, V. D. *Acc. Chem. Res*. **1993**, *26*, 287.

(4) (a) Kern, J. M.; Federlin, P. *Tetrahedron* **1978**, *34*, 661. (b) Bordwell, F. G.; Bausch, M. J. *J. Am. Chem. Soc.* **1986**, *108*, 1979. (c) Bordwell, F. G.; Bausch, M. J. *J. Am. Chem. Soc.* **1986**, *108*, 1985.

(5) (a) Andrieux, C. P.; Hapiot, P.; Pinson, J.; Savéant, J.-M. *J. Am. Chem. Soc*. **1993**, *115*, 7783. (b) Lund, T.; Pedersen, S. U. *J. Electroanal. Chem*. **1993**, 362, 109.

(6) (a) Andrieux, C. P.; Grzeszczuk, M.; Savéant, J.-M. *J. Am. Chem. Soc.* **1991**, *113*, 8811. (b) Andrieux, C. P.; Grzeszczuk, M.; Savéant, J.-M. *J. Electroanal. Chem*. **1991**, 318, 369.

(7) (a) Andrieux, C. P.; Savéant, J.-M. In *Electrochemical Reactions in Investigation of Rates and Mechanisms of Reactions, Techniques of Chemistry*; Bernasconi, C. F., Ed.; Wiley: New York, 1986; Vol. VI/4E, Part 2, pp 305−390. (b) Andrieux, C. P.; Hapiot, P.; Savéant, J.-M. *Chem. Rev*. **1990**, *90*, 723.

(8) (a) Fuhlendorf, R.; Occhialini, D.; Pedersen, S. U.; Lund, H. *Acta Chem. Scand*. **1989**, *43*, 803. (b) Lund, H.; Daasbjerg, K.; Occhialini, D.; Pedersen, S. U. *Russ. J. Electrochem.* **1995**, *31*, 865. (c) Lund, H.; Daasbjerg, K.; Lund, T.; Occhialini, D.; Pedersen, S. U. *Acta Chem. Scand*. **1997**, *51*, 135.

(9) (a) Nadjo, L.; Savéant, J.-M.; Su, K. B. *J. Electroanal. Chem*. **1985**, 196, 23. (b) Pedersen, S. U. *Acta Chem. Scand. A* **1987**, *41*, 391.

(10) (a) Wayner, D. D. M.; Griller, D. *J. Am. Chem. Soc.* **1985**, *107*, 7764. (b) (a) Wayner, D. D. M.; McPhee, D. J.; Griller, D. *J. Am. Chem. Soc*. **1988**, *110*, 132. (c) Griller, D.; Wayner, D. D. M. *Pure Appl. Chem.* **1989**, *61*, 754. (d) Nagaoka, T.; Griller, D.; Wayner, D. D. M. *J. Phys. Chem*. **1991**, 95, 6264. (e) Wayner, D. D. M.; Houmam, A. *Acta Chem. Scand*. **1998**, *52*, 377.

(11) Smith, K. D.; Strohben, W. E.; Evans, D. H. *J. Electroanal. Chem*. **1990**, 288, 111.

S0002-7863(98)01801-0 CCC: $15.00
Published on Web 09/17/1998

RX, according to Scheme 1.

Scheme 1

$$P + e^-(\text{electrode}) \rightleftharpoons Q^{\bullet -}$$

$$RX + Q^{\bullet -} \rightarrow R^{\bullet} + X^- + P$$
(in one step or in two steps)

$$R^{\bullet} + Q^{\bullet -} \xrightarrow{k_{ET}} R^- + P$$

$$R^{\bullet} + Q^{\bullet -} \xrightarrow{k_{coupling}} RQ^-$$

Using, for example, linear scan voltammetry, the cathodic peak current (normalized to its value in the absence of RX) is a function of the ratio $k_{ET}/k_{coupling}$.[9] k_{ET} can be varied using a series of more and more reducing mediators so as to reach eventually the bimolecular diffusion limit. $k_{coupling}$ seems to be about constant in series of aromatic anion radicals and lower than the bimolecular diffusion limit. Plotting of the ratio $k_{ET}/(k_{ET} + k_{coupling})$ leads to a "polarogram" of the radical whose half-wave potential provides the potential where $k_{ET} = k_{coupling}$ and, therefore, the value of k_{ET} for this value of the potential, provided $k_{coupling}$ is known independently (the various assumptions under which the rate data are analyzed and the necessity of an independent estimation of $k_{coupling}$ limit the applicability and accuracy of the method). The derivation of the standard potential from the value of k_{ET} thus obtained requires the application of an activation/driving force relationship (derived, e.g., from Marcus theory) and an independent estimation of the intrinsic barrier.

Two photoelectrochemical methods have been proposed for investigating the reduction characteristics of transient free radicals. In one of them,[10] the radical is generated by photolysis of a labile substrate with modulated light. The reduction current of the radical at a minigrid electrode, whose potential can be controlled independently, varies periodically with time at the frequency of the modulated light and can be recorded at any value of the phase lag between light and current. Finite difference simulation of the in-phase and out-of-phase current potential curves with a reaction scheme involving, besides electron transfer at the electrode, dimerization of the radical and follow-up reactions of the anion (or cation in the case of an oxidation) has allowed the determination of the various rate parameters and of the radical standard potential, at least in the case of the reduction (and oxidation) of the diphenylmethyl radical in acetonitrile.[10d] One may also produce the radical by continuous irradiation and use fast electrochemical techniques, such as normal and reverse pulse voltammetry at an ultramicroelectrode, to obtain the radical standard potential, at least in favorable cases, such as the oxidation of the diphenylmethyl radical and the reduction of the diphenylcyanomethyl radical.[11] One limitation of the method is the possible superposition of large photocurrents arising from the photoinjection of electrons from the electrode into the solution.[12]

The exploitation of the latter phenomenon is the basis of the electron photoinjection method.[12b] The radical-generating molecule is photostable at the wavelength selected to photoeject the electrons from the electrode by means of a laser pulse. The radical is produced by reduction of a rapidly or concertedly cleaving substrate RX by the thermalized photoinjected electrons. Thus, shortly after the end of the laser pulse, a thin layer (of the order of 30−100 Å thick) of radicals (surface concentration of the order of 10^{-13} mol/ cm^2) has built up at the electrode surface. The variation of the photoinduced charge flowing through the electrode with the electrode dc potential allows the construction of a polarogram of the radical which represents its reduction into the corresponding carbanion. The half-wave potential is a measure of the reducibility of the radical, but, here again, the standard potential of the radical/anion couple cannot be equated with the half-wave potential in most cases.

We have established elsewhere the theoretical expressions that relate the half-wave potential and shape of the radical polarograms to the thermodynamics and kinetics of the various reactions in which the radical and the anion resulting from its reduction may be engaged.[13] In the work reported below, we have applied the ensuing mechanism diagnostic criteria and reactivity determination procedures to the reduction of a series of arylmethyl radicals. The 9-anthrylmethyl, diphenylmethyl, benzyl, and 4-methylbenzyl radicals were generated by reduction of the corresponding chlorides by electrons photoinjected in laser pulse experiments. The variation of the half-wave potential with the measurement time was the main source of mechanism and reactivity information, and the shape of the polarograms was used as an additional diagnostic criterion. Addition of acids into the solution, insofar as it accelerates the disappearance of the carbanion, provided further insight into the reaction mechanism. The results are compared with earlier data obtained by other techniques, when available, and the reactivity parameters are discussed with the help of density functional quantum chemical calculations.

Results

Most experiments were carried out at 20 °C in *N*,*N*′-dimethylformamide (DMF) with Et_4NClO_4 as supporting electrolyte. The working electrode was a gold disk. These experimental conditions appear to be the most satisfactory in terms of reproducibility. A few test experiments were, nevertheless, performed with *n*-Bu_4NPF_6 as electrolyte and acetonitrile as solvent for comparing our results with earlier data obtained by application of the photolytic and redox catalysis techniques. The polarograms, i.e., the plots of the apparent fraction of electron, *n*, consumed in the reduction of the radical versus the dc electrode potential, *E*, were extracted from the raw charge injection data as described in section 1 of ref 13.

9-Anthrylmethyl. We start with the reduction of 9-anthrylmethyl chloride, for which the determination of all the thermodynamic and kinetic parameters is the easiest. Figure 1a and b shows typical polarograms recorded at each end of the time window (7 and 500 μs, respectively). Figure 1c displays the variation of the half-wave potential, $E_{1/2}$, with the measurement time, *t*, over the whole time window. The shape of this curve, particularly the presence of an inflection in the middle of the time window, is typical of the kinetic influence of the electron-transfer step and of a relatively slow follow-up reaction (see Figure 7 in ref 13), most probably a reaction of the anion with acids present in the medium. One should also take into account the dimerization of the radical, which is expected to be a fast reaction. As discussed earlier, the effect of this reaction is to diminish the slope of the $E_{1/2}$ vs log *t* plot, more for longer times than for short times (see Figure 19 in ref 13). This picture is confirmed by the changes observed upon addition of an acid, phenol, into the solution (Figure 1c). The result is a general positive shift of the half-wave potential, which is larger at long times than at short times, while the inflection progressively

(12) (a) Hapiot, P.; Savéant, J.-M., unpublished results. (b) Hapiot, P.; Konovalov, V. V.; Savéant, J.-M. *J. Am. Chem. Soc.* **1995**, *117*, 1428 and references therein.

(13) Gonzalez, J.; Hapiot, P.; Konovalov, V. V.; Savéant, J.-M., submitted.

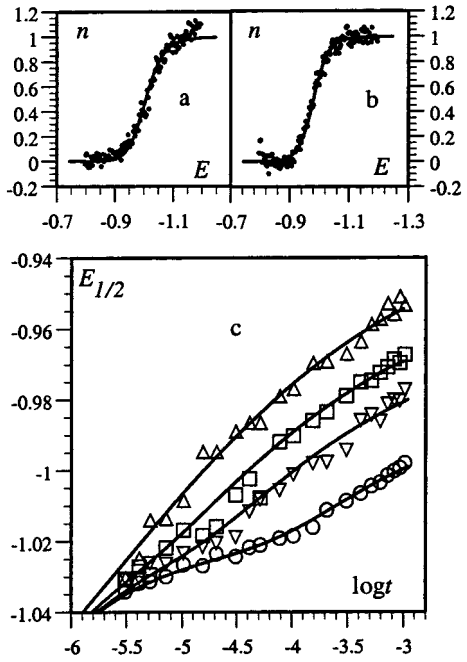

Figure 1. Reduction of 9-anthrylmethyl chloride (1 mM) by laser pulse photoinjected electrons in DMF + 0.1 M Et_4NClO_4. (a, b) Polarograms of the 9-anthrylmethyl radical at 7 and 500 μs, respectively. (c) Variation of the half-wave potential with the measurement time in the absence (○) and presence of 0.25 (▽), 0.5 (□), and 2 (△) mM phenol. The potentials are in volts vs SCE. The full lines are simulated curves (see text).

disappears. These observations are consistent with Scheme 2, where E^0, α, and k_S are the standard potential, transfer coefficient, and standard rate constant of electron transfer, respectively, and $k = k_0 + k_{PhOH}[PhOH]$.

Scheme 2

$$R{-}R \xleftarrow{2k_d} 2R^{\bullet}$$

$$R^{\bullet} + e^{-} \underset{\alpha,\, k_S}{\overset{E^0}{\rightleftharpoons}} R^{-}$$

$$R^{-} \xrightarrow{k_0} \text{products}$$

$$R^{-} + PhOH \xrightarrow{k_{PhOH}} RH + PhO^{-}$$

The fact that the positive shift of $E_{1/2}$ is larger at long times than at short times, where it vanishes, results from the tendency for the follow-up reaction to control the kinetics in the former conditions, whereas the forward electron-transfer step becomes rate-determining in the latter conditions. Since, as seen below, the reduction potential of the radical is not far from its standard potential, we may assume that $\alpha = 0.5$. Finite difference simulation of the polarograms according to the procedure depicted in section 6 and Appendix IV of ref 13, allows the fitting of the $E_{1/2}$ vs log t plots with the values of E^0, k, k_S, and $2k_d$ reported in Table 1. The adjustment of the value for $2k_d$ is, in fact, better performed with the highest concentration of phenol after the inflection has disappeared. The inclusion of the dimerization reaction in the reaction scheme according to which the simulations are carried out requires the value of $\Gamma°$, the amount of radical initially generated from the capture of the solvated electrons by 9-anthrylmethyl chloride. $\Gamma°$ was found to be equal to 8.7×10^{-14} mol cm^{-2} using the procedure described in section 1 of ref 13. As long as the $E_{1/2}$ vs log t plot exhibits an inflection, a full finite difference fitting of the

Table 1. Thermodynamic and Kinetic Parameters[a]

radical	$2k_d$[b] ($\times 10^9$ M^{-1} s^{-1})	E^0[c] (V vs SCE)	k_0[d] ($\times 10^4$ s^{-1})	k_{PhOH}[e] ($\times 10^8$ M^{-1} s^{-1})	k_S[f] (cm s^{-1})	λ_{elec}[g] (eV)
9-anthrylmethyl	3	−1.018	1	4	2.0	0.782
diphenylmethyl	2	−1.107	30	2	4.5	0.702
benzyl	8	−1.215	5	2	0.7	0.925

	$2k_d$[b] ($\times 10^9$ M^{-1} s^{-1})	$\frac{k^{\alpha/(1-\alpha)}D^{1/(1-\alpha)}}{k_S^{2/(1-\alpha)}}$	$E^0 + (RT/2F)\ln k$	$E^0 + (RT/\alpha F)\ln k_S$
benzyl[h]	8	∞		−1.467
4-methylbenzyl	6	10^{-5}	−1.175	−1.320

[a] At 20 °C, in DMF + 0.1 M Et_4NClO_4, unless otherwise stated. [b] Dimerization rate constant. [c] Standard potential of the radical/anion couple. [d] Rate constant of the follow-up reaction with no acid added. [e] Bimolecular rate constant of the reaction of the anion with phenol. [f] Electron-transfer standard rate constant, $\alpha = 0.5$ unless otherwise stated. [g] Reorganization free energy of the electrochemical electron transfer, computed from $k_S \cong Z_{elec} \exp(-F\lambda_{elec}/4RT)$, with $Z_{elec} = (RT/2\pi M)^{1/2} = 4.6$-, 4.7-, and 6.6×10^3 cm s^{-1}, respectively. [h] In acetonitrile + 0.1 M n-Bu_4NPF_6, $\alpha = 0.4$.

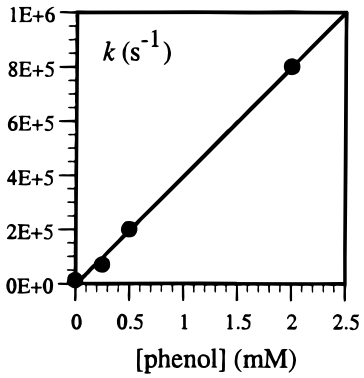

Figure 2. Neutralization of the 9-anthrylmethyl carbanion with phenol. Variation of the pseudo-first-order rate constant with the phenol concentration.

experimental points is necessary. When the inflection has disappeared, after addition of enough phenol, the fitting curves can be derived from a single working curve (see Figures 16 and 18 in section 6 of ref 13). The resulting values of E^0, $2k_d$, k_S, and k_0 (the rate constant of the follow-up reaction in the absence of phenol) are gathered in Table 1. Simulation of the whole individual polarogram confirms the assignment of the reaction mechanism. Two typical examples are shown in Figure 1a and b, corresponding to each end of the time window.

The variation of the rate constant of the follow-up reaction with the concentration of phenol is displayed in Figure 2. As expected, the variation is linear:

$$k = k_0 + k_{phenol}[PhOH]$$

The slope of this linear plot provides the rate constant of the second-order reaction of the anion with phenol (Table 1).

Diphenylmethyl. In this case, too, the half-wave potential shifts positively upon addition of phenol (Figure 3), suggesting a similar reduction mechanism. There are, however, significant differences between the $E_{1/2}$ vs log t plots in the diphenylmethyl and 9-anthrylmethyl cases. The inflection observed in the absence of phenol is less apparent than that with the 9-anthrylmethyl radical, indicating that the follow-up reaction is faster. It is also remarkable that, in the presence of phenol, the slopes of the $E_{1/2}$ vs log t curves indicate that the reduction is controlled almost completely by the follow-up reaction, with only a modest kinetic interference of the electron-transfer step. This observation falls in line with the fact that the vertical distance between

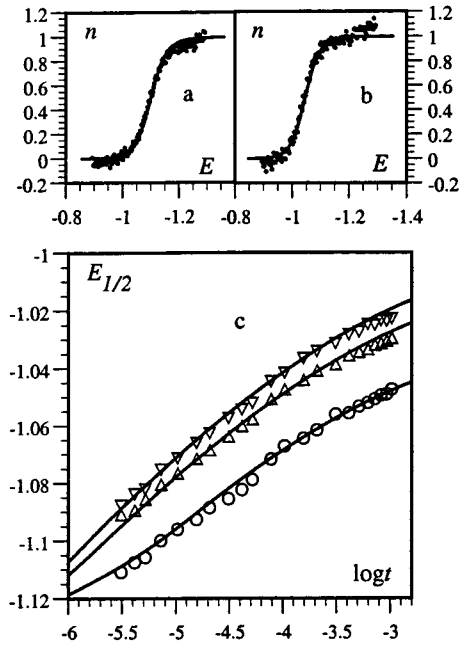

Figure 3. Reduction of diphenylmethyl chloride (30 mM) by laser pulse photoinjected electrons in DMF + 0.1 M Et_4NClO_4. (a, b) Polarograms of the diphenylmethyl radical at 7 and 500 μs, respectively. (c) Variation of the half-wave potential with the measurement time in the absence (○) and presence of 10 (△) and 20 (▽) mM phenol. The potentials are in volts vs SCE. $\Gamma^0 = 10^{-13}$ mol cm^{-2}. The full lines are simulated curves (see text).

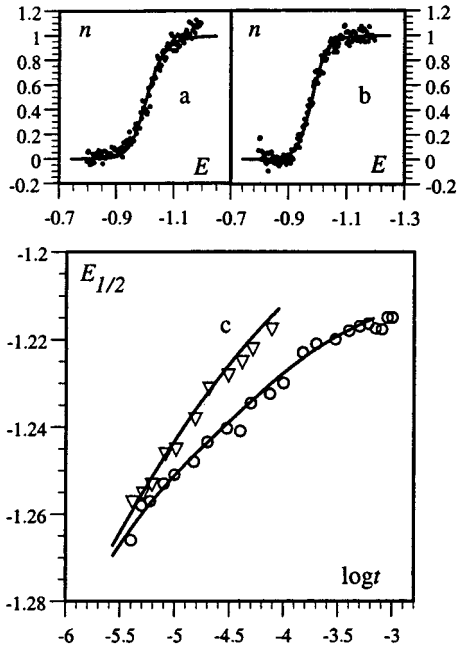

Figure 4. Reduction of benzyl chloride (10 mM) by laser pulse photoinjected electrons in DMF + 0.1 M Et_4NClO_4. (a, b) Polarograms of the benzyl radical at 7 and 500 μs, respectively. (c) Variation of the half-wave potential with the measurement time in the absence (○) and presence of 5 (▽) mM phenol. The potentials are in volts vs SCE. $\Gamma^0 = 10^{-13}$ mol cm^{-2}. The full lines are simulated curves (see text).

the curves is almost constant from the left to the right end of the time window, being only slightly smaller in the first case than in the second. Since the follow-up reaction is faster than that with the 9-anthrylmethyl radical and, at the same time, the kinetic interference of the electron-transfer step is weak, we expect the standard rate constant to be larger. This is, indeed, what appears from the fitting of the $E_{1/2}$ vs log t plots. The resulting values of E^0, k_0, k_S, and $2k_d$ are listed in Table 1. The variation of k with the phenol concentration is again linear, leading to the value of k_{phenol} reported in Table 1. The shapes of the polarograms again provide a satisfactory confirmation of the reaction mechanism. There is, indeed, a good agreement between the experimental and simulated polarograms, as illustrated by the two examples, taken at each end of the time window, which are represented in Figure 3a and b.

Benzyl. Typical polarograms and $E_{1/2}$ vs log t plots are shown in Figure 4. They exhibit the same general feature as in the preceding cases. The right-hand side of the $E_{1/2}$ vs log t plot is, however, flatter, indicating that the dimerization of the radical is faster. The inflection is much less apparent than that with the 9-anthrylmethyl radical, indicating that the follow-up reaction is faster. The fact that the $E_{1/2}$ vs log t plot obtained upon addition of phenol converges with the plot obtained without phenol at the lower end of the time window indicates that the electron-transfer step becomes rate-determining under these conditions. In the presence of phenol, meaningful results cannot be obtained at the upper end of the time window. This is presumably due to the fact that some phenol is reduced by the solvated electrons simultaneously with benzyl chloride. That this phenomenon is not observed with anthrylmethyl and diphenylmethyl chlorides, which are reduced at more positive potentials than benzyl chloride (the cyclic voltammetric peak potentials of the chlorides, on a gold disk electrode at 0.2 V/s, are −1.38, −1.89, and −2.19 V vs SCE respectively), confirms this interpretation. As seen further on, the same observation was made in acetonitrile in the absence of phenol, which can be explained within the same framework, since acetonitrile, being easier to reduce than DMF, may well capture the solvated electrons concurrently with benzyl chloride. The values of the various thermodynamic and rate parameters derived from the fitting of the experimental points shown in Figure 4 are listed in Table 1. We also checked that the slopes of the individual polarograms agree with the reaction mechanism and the values of the various parameters (two illustrative examples are given in Figure 4a and b).

Although we currently carried out most experiments with Et_4NClO_4 as supporting electrolyte, we performed a test experiment with n-Bu_4NPF_6 for comparison with earlier data derived from the photolytic[10] and redox catalysis techniques.[8] No significant differences were found between the two electrolytes.

Acetonitrile, rather than DMF, was used in previous photolytic studies.[10] Acetonitrile gives rise to larger background currents in EPI experiments because it is a better scavenger of the photoinjected electrons. At the price of some limitation of the time window toward its upper end, we carried out an experiment in acetonitrile in order to unravel the intriguing observation that the reduction potential of benzyl radical is reported to be ca. 200 mV more negative than what we find in DMF (Figure 4). Rather than benzyl chloride, we used the more reducible benzyl bromide to improve the fraction of photoinjected electrons captured by the substrate rather than by the solvent. Figure 5 shows our results. It appears that the reduction potential is about 200 mV more negative in acetonitrile than in DMF, thus reaching values that are in agreement with the value found by the photolytic technique.[10] Another difference with DMF is that electron transfer is the rate-determining step over the whole available time window, thus masking the effect of the follow-up reaction. This observation indicates that the electron transfer is slower and/or the follow-up reaction faster in acetonitrile than in DMF. Under these conditions, the standard potential cannot be rigorously derived from the $E_{1/2}$

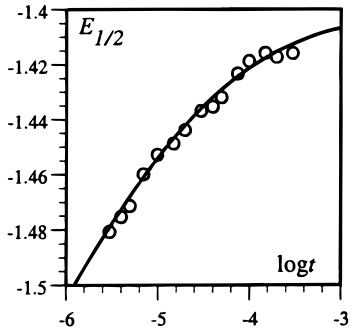

Figure 5. Reduction of benzyl bromide (30 mM) by laser pulse photoinjected electrons in acetonitrile + 0.1 M *n*-Bu_4NNPF_6. Variation of the half-wave potential with the measurement time. $\Gamma^0 = 2.2 \times 10^{-13}$ mol cm^{-2}.

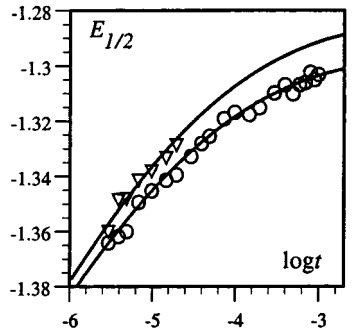

Figure 6. Reduction of 4-methylbenzyl chloride (10 mM) by laser pulse photoinjected electrons in DMF + 0.1 M Et_4NClO_4. Variation of the half-wave potential with the measurement time in the absence (○) and presence of 5 (▽) mM phenol. $\Gamma^0 = 1.13 \times 10^{-13}$ mol cm^{-2}.

vs log t plot. What can be obtained is a reduction potential combining the standard potential, the transfer coefficient, and the standard rate constant. Fitting of the experimental points with the appropriate working curve (Figure 15 and eq 143 in ref 13), as shown in Figure 5, leads to the determination of $2k_d$, α, and $E^0 + (RT/\alpha F) \ln k_S$ (Table 1).

4-Methylbenzyl. Figure 6 shows the $E_{1/2}$ vs log t plots obtained in the absence of and in the presence of phenol. In the latter case, we observe the same inaccessibility of the long measurement times as with benzyl chloride (4-methylbenzyl chloride is even more difficult to reduce than benzyl chloride, with a peak potential of −2.21 V vs SCE, on a gold disk electrode at 0.2 V/s). The follow-up reaction is now so fast that no trace of inflection can be detected in the $E_{1/2}$ vs log t plot. The slope of the plots and their small separation indicate that electron transfer almost completely controls the reduction reaction of the radical, in competition with dimerization. Thus, the electron transfer is slower and/or the follow-up reaction faster with the 4-methylbenzyl radical than with the benzyl radical. Fitting of the experimental points, as shown in Figure 6, leads to the determination of $2k_d$, α, $k^{\alpha/(1-\alpha)}D^{1/(1-\alpha)}/k_S^{2/(1-\alpha)}$, $E^0 + (RT/2F) \ln k$, and $E^0 + (RT/\alpha F) \ln k_S$ (Table 1).

For each compound, the constants in Table 1 were derived from the consistent analysis of all the $E_{1/2}$ vs log t plots obtained in the absence of and in the presence of phenol, with the same values of the standard potential, transfer coefficient, and standard rate constant of electron transfer. Repeated simulations then showed that the uncertainty on rate constants is less than 50% and is about ±5 mV on the potentials.

Discussion

Among the results gathered in Table 1, the values of the radical dimerization rate constants are consistent with literature data.[10d] Concerning the characteristics of the electron-transfer step, we may first compare our results to those previously obtained by the photolytic technique in acetonitrile.[10b−d] The half-wave potentials we find in DMF for the benzyl radical are about 200 mV more positive than the half-wave potential found in acetonitrile by the photolytic technique.[10] However, the checking EPI experiment we carried out in acetonitrile gave half-wave potentials that are in agreement with the latter value. Thus, there is no real discrepancy between the two techniques. In acetonitrile, the EPI experiments have shown that the rate-determining step is the forward electron transfer (in competition with radical dimerization), while, in DMF, there is a mixed kinetic control involving both the electron transfer and the follow-up reaction. The same should be true with the photolytic technique. The exact nature of the follow-up reaction taking place in the absence of phenol is not known. It seems likely to involve Lewis and/or Brönsted acids present in the reaction medium. A test experiment where the concentration of supporting electrolyte was increased from 20 mM to 0.2 M did not show any significant variation of the $E_{1/2}$ vs log t plot, thus ruling out the involvement of the Brönsted acid properties of the tetraalkylammonium. We may, therefore, conclude that the solvent itself is involved as a Lewis acid. Because acetonitrile is more acidic than DMF, we expect the standard potential to be more positive, the follow-up reaction to be faster, and the standard rate constant of electron transfer to be smaller in acetonitrile than in DMF.[14] The combination of the latter two factors explains why electron transfer is the rate-determining step in acetonitrile, whereas electron transfer and the follow-up reaction jointly govern the kinetics in DMF.

If we compare our results with those of the redox catalysis technique in DMF, it appears that the standard potential we find for the benzyl radical, −1.215 V vs SCE, is significantly more positive than the value derived from redox catalysis, −1.40 V vs SCE,[8] which is, itself, close to the photolytic half-wave potential in acetonitrile.[10] The significant differences in half-wave potentials and kinetic control we have found between the two solvents suggest that the standard potentials should also be different. The redox catalysis data were analyzed in the framework of Scheme 1, where the forward electron-transfer step is irreversible, assuming a rather small value of the self-exchange reorganization free energy, λ_{se} (0.433 eV). As shown below, our results and the redox catalysis data may be reconciled using a larger value of λ_{se}, which seems more likely in view of the electrochemical kinetic data and of a quantum chemical estimate. With the mediator ($E^0_{P/Q} = -1.42$ V vs SCE) corresponding to the redox catalysis "half-wave potential", $k_e = k_{coupling} = 10^9$ M^{-1} s^{-1}. Our value of the standard potential implies that the cross-exchange reorganization free energy λ is equal to 0.94 eV, as results from the application of the following equations.

$$\Delta G_e^{\ddagger} = \frac{\lambda}{4}\left(1 + \frac{E^0_{P/Q} - E^0}{\lambda}\right)^2, \quad k_e = Z \exp\left(-\frac{F\Delta G_e^{\ddagger}}{RT}\right)$$

where $\Delta G_e^{\ddagger}$ is the activation free energy of electron transfer, and $Z = 6.6 \times 10^{11}$ M^{-1} s^{-1} is the bimolecular collision frequency. Since $\lambda = (\lambda_{se} + \lambda_{ed})/2$, (λ_{ed} are the self-exchange reorganization free energies of the electron donor), λ_{se} may be

(14) (a) It has previously been observed that solvent reorganization is larger in acetonitrile than in DMF in the reduction of stable organic compounds[14b] and, more generally, that it increases with the acceptor number of the solvent.[14c] (b) Savéant, J.-M.; Tessier, D. *J. Electroanal. Chem.* **1975**, 65, 57.(c) Fawcett, W. R.; Jaworski, J. S. *J. Phys. Chem.* **1983**, *87*, 2972.

estimated as equal to 1.24 eV.[15] As will be shown further on, the latter value is close to what quantum chemical calculations predict. This value of λ_{se} is significantly larger than the value previously assumed.[8] For the reasons given below, it is also consistent with the kinetics of the electrochemical reduction of the radical. The electrochemical reorganization free energy is estimated as $\lambda_{elec} = 0.925$ eV from the standard rate constant of electron transfer, uncorrected for double-layer effects. From previous data on the electrochemical reduction of a series of aromatic molecules in DMF,[15b] it appears that the solvent reorganization free energy derived from double-layer corrected data falls between the predictions of Marcus's model (where image effects are taken into account)[16a,b] and Hush's model (where they are not).[16c,d] The latter model thus predicts that the electrochemical and homogeneous self-exchange reorganization free energies are the same. Starting from data that are uncorrected for double-layer effects, λ_{elec} is found to be slightly smaller than Hush's predictions, thus leading to $\lambda_{elec} = 0.89\lambda_{se}$.[15c] If we assume that the double-layer effect is about the same at a mercury electrode where the aromatic molecule data were gathered and at the gold electrode with which we obtained the benzyl radical data, it follows that λ_{se} should be of the order of 1.04 eV (24 kcal mol^{-1}), more than twice the value used in the previous analysis of the redox catalysis data. An additional confirmation of the above analysis stems from the consideration of the role of the follow-up reaction in the kinetics of the redox-catalyzed reaction, replacing the irreversible electron-transfer step in Scheme 1 by the following two reactions.

$$R^{\bullet} + Q^{\bullet -} \underset{k_{-e}}{\overset{k_e}{\rightleftharpoons}} R^- + P, \quad R^- \xrightarrow{k_0} \text{products}$$

With a value of λ_{se} as small as 0.433 eV, the follow-up reaction is expected to be the rate-determining step, whereas with λ_{se}= 1.24 eV, the rate-determining step is the forward electron transfer.[17]

For the diphenylmethyl radical, the standard potential we find, −1.107 V vs SCE, is much closer to the value derived from redox catalysis experiments, −1.07 V vs SCE. The electrochemical electron transfer is very fast, corresponding to a small electrochemical reorganization free energy, 0.7 eV. Rough estimates of λ_{se} and λ are 0.8 and 0.7 eV, respectively, pointing to a possible involvement of the follow-up reaction in the kinetics of the redox catalytic reduction besides the electron-transfer step ($k_{-e}C_p^0/k_0$ is of the order of 2).

To help chemical intuition in interpreting the thermodynamic and kinetic data summarized in Table 1, we performed a series of quantum mechanical calculations. We selected a density functional approach as a compromise between accuracy and calculation time. This approach is expected to provide more reliable results than semiempirical and simple Hartree−Fock techniques, especially with open-shell molecules, while it remains tractable with the relatively large molecules we are dealing with. The results thus obtained are summarized in Table 2.

Table 2. Quantum Chemical Estimations[a]

	radical	benzyl	diphenyl-methyl	anthryl-methyl
solvation G^0_{solv} [b]	R^-	−2.43	−2.15	−2.10
	$R^{\bullet}$	−0.08	−0.13	−0.13
	RH	−0.08	−0.15	−0.13
$R^{\bullet} + e^- \rightleftharpoons R^-$	$-\Delta U^0_{el}$ [c]	0.17	0.84	0.95
	$-(\Delta U^0_{el} + \Delta G^0_{solv})$	2.51	2.86	2.92
	$-\Delta G^0$ [d]	2.58		
	$\lambda_{0,elec}$	1.21	1.07	1.05
	$\lambda_{i,elec}$[18]	0.07	0.08	0.05
$R^- + PhOH \rightleftharpoons$	ΔU^0_{el} [c]	−1.94	−0.86	−0.88
$RH + PhO^-$	$\Delta U^0_{el} + \Delta G^0_{solv}$	−2.06	−1.32	−1.36
	ΔG^0 [d]	−2.01	−1.32	

[a] Energies in eV. [b] Solvation free energy. [c] Variation of the electronic energy. [d] Includes the electronic, zero-point, and thermal energies and the entropic term (at 20 °C).

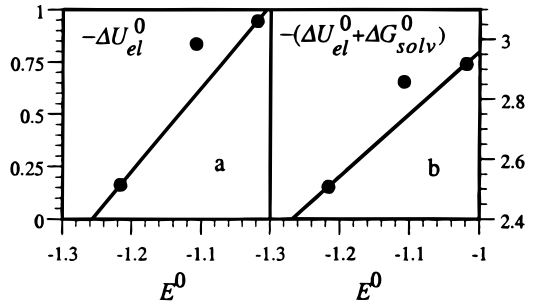

Figure 7. Correlation of the variation in electronic energy (a) and the variation of the sum of the electronic energy and the solvation free energy (b) with the experimental standard potential. Energies in electronvolts, potential in volts vs SCE.

Both the benzyl radical and the benzyl anion are planar, while the diphenylmethyl and anthrylmethyl radicals and anions are slightly distorted. The geometry, charge distribution, and energy data for these species and the corresponding hydrocarbons are given in the Supporting Information.

In agreement with experiments and intuition, the calculations indicate that the standard potential shifts positively from the benzyl to the diphenylmethyl and anthrylmethyl radicals. Figure 7a shows the correlation between the experimental standard potential and the variation of the electronic energy, $-\Delta U^0_{el}$, from the anion to the radical. The variations of the two quantities are parallel, but the variation of the electronic energy term is much more rapid than the variation of the experimental E^0 (the slope is close to 4). In Figure 7b, the correlation takes into account the solvation free energy upon passing from the anion to the radical. This term was calculated according to the

(15) (a) Taking $\lambda_{ed} = 0.64$ eV.[15b] (b) Kojima, H.; Bard, A. J. *J. Am. Chem. Soc*. **1975**, *97*, 6317. (c) Andrieux, C. P.; Savéant, J.-M.; Tardy, C. *J. Am. Chem. Soc*. **1998**, *120*, 4167.

(16) (a) Marcus, R. A. *J. Chem. Phys*. **1956**, *24*, 966. (b) Marcus, R. A. *J. Chem. Phys*. **1956**, *24*, 979. (c) Hush, N. S. *J. Chem. Phys*. 1958, *28*, 962. (d) Hush, N. S. *Trans Faraday Soc*. **1961**, *57*, 557. (e) Marcus, R. A. *J. Chem. Phys*. **1965**, *43*, 679.

(17) The kinetic competition between electron transfer and follow-up reaction is a function of the dimensionless parameter $k_{-e}C_p^0/k_0$, where C_p^0 is the concentration of mediator. From the standard potential of the mediator corresponding to the "half-wave" potential, −1.42 V vs SCE, and a value of the standard potential of the radical equal to −1.40 V vs SCE (corresponding to λ_{se}= 0.433 eV), one obtains $k_{-e} = 5 \times 10^8$ M^{-1} s^{-1}. With $C_p^0 = 2 \times 10^{-3}$ M, and k_0 from Table 1, it is found that $k_{-e}C_p^0/k_0 = 20$ ($\gg$1), indicating that the follow-up reaction is the rate-determining step. The standard potential of the radical is equal to −1.215 V vs SCE (corresponding to λ_{se}= 1.24 eV), $k_{-e} = 3 \times 10^5$ M^{-1} s^{-1}, and thus $k_{-e}C_p^0/k_0 = 0.01$ ($\ll$1), indicating that the redox-catalyzed reduction is under the kinetic control of the forward electron transfer.

(18) (a) λ_i is obtained from the difference in energy between the radical at its equilibrium geometry and at the equilibrium geometry of the anion and, conversely, from the difference in energy between the anion at its equilibrium geometry and at the equilibrium geometry of the radical. For homogeneous self-exchange reactions, λ_i is the sum of these two energies,[17b] while it is the half-sum for electrochemical reactions.[16] The two energies thus obtained were found to be almost the same for all three radicals, 0.075 and 0.078 for benzyl, 0.075 and 0.084 for diphenylmethyl, 0.051 and 0.052 for anthrylmethyl. (b) Klimkans, A.; Larsson, S. *Chem. Phys*. **1994**, *189*, 25.

charge isodensity method, optimization of the geometry being performed in the gas phase.[19] The variations are again parallel, but, although improved, the slope of the correlation, 2, is still well above 1. Possible causes of this overestimation of the variation of the standard potential are as follows. It may result from the optimization of the geometry being performed in the gas-phase rather than in the solvent. Another reason may be the neglect of the discreteness of the solvent. A third factor is the stabilizing interaction of the anion with the cation of the supporting electrolyte, which is expected to decrease with the concentration of the negative charge, i.e., from the benzyl to the diphenylmethyl and anthrylmethyl radicals.

It is noteworthy that the diphenylmethyl data point stands above the correlation lines (Figure 7), suggesting that the diphenylmethyl anion is relatively less solvated (and interacts relatively less with the countercation) that the two other anions. A possible reason for this behavior is a lesser accessibility, caused by steric hindrance, of the negative charge borne by the benzylic carbon (see the molecular structures in the Supporting Information).

Regarding electrochemical kinetics, the Marcus−Hush model[16] divides the attending reorganization free energy into a solvent reorganization term, $\lambda_{0,elec}$, and an intramolecular reorganization term, $\lambda_{i,elec}$. Estimation of $\lambda_{i,elec}$[18] shows that it is much smaller than $\lambda_{0,elec}$ (Table 2). The solvent reorganization free energy for the homogeneous self-exchange reaction, $\lambda_{0,se}$ may be derived from $-\Delta G^0_{solv}$ by multiplication by $(1/D_{op} - 1/D_S)/(1 - 1/D_S)$, where $D_{op} = 2.04$ is the optical dielectric constant, and $D_S = 36.7$ is the static dielectric constant in DMF.[20] In Hush's model, the reaction site is assumed to be far enough from the electrode surface for the image force and double layer effects to be neglected. It is thus expected that $\lambda_{elec} = \lambda_{0,se} + \lambda_{i,elec}$, where λ_{elec} is directly derived from the raw kinetic data with no correction of the double-layer effect. In Marcus's model, the reaction is assumed to take place when the reactant is in close contact with the electrode surface. Thus, $\lambda_{elec} = \lambda_{0,se}/2 + \lambda_{i,elec}$, where λ_{elec} is derived from the kinetic data after correction of the double-layer effect, which, in the case of the formation of an anion from a neutral molecule, is expected to increase the rate constant by ca. 1 order of magnitude and thus to decrease $\lambda_{0,elec}$ by ca. 0.24 eV. As discussed earlier, data pertaining to the reduction of an extended set of aromatic molecules on mercury are close to the prediction of Hush's model, namely $\lambda_{elec} = 0.89\lambda_{se}$. It thus seems natural to attempt, in the present case, a correlation between the theoretical values of $\lambda_{theor} = \lambda_{0,se}\ \lambda_{i,elec}$ and the experimental values of λ_{elec}, λ_{exp}, derived from the raw kinetic data with no correction of the double-layer effect. Figure 8 shows the correlation between these two quantities. For the benzyl and anthrylmethyl radicals, there is a good correlation corresponding to $\lambda_{elec} = 0.72\lambda_{se}$, which seems reasonable taking into account the uncertainty in the estimation of double-layer effects on gold, as compared to mercury, and the fact that the location of the reaction site for the present radicals is not necessarily the same as for aromatic molecules. In contrast, the reduction of the diphenylmethyl radical is significantly faster than predicted theoretically. This anomaly, which we have already observed with the standard potentials, may be explained along the same lines, namely, a lesser accessibility of the solvent to the negative charge borne by the benzylic carbon in the diphenylmethyl anion as compared to the two other radicals.

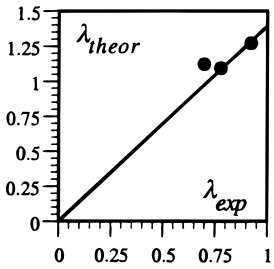

Figure 8. Kinetics of electron transfer. Correlation between the theoretical and experimental (see text) reorganization free energies (in eV).

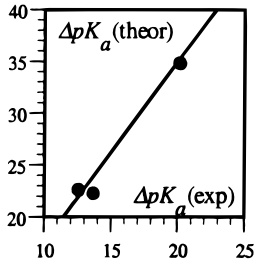

Figure 9. Correlation between the theoretical (see text) and experimental pK_as of the benzyl, diphenylmethyl, and anthrylmethyl anion, referenced to the pK_a of phenol (18.8) in DMF.

We now discuss the kinetics of *protonation* of the benzyl, diphenylmethyl, and anthrylmethyl anions. It is remarkable that the protonation rate constants of the three anion are practically the same ($(2-5) \times 10^8$ M^{-1} s^{-1}), while being clearly below the diffusion limit (10^{10} M^{-1} s^{-1}). The pK_as of the diphenylmethyl and anthrylmethyl anions have been measured in dimethyl sulfoxide (DMSO) and found to be 32.25 and 31.1, respectively,[21a] which translate into 32.5 and 31.4 in DMF.[21b] For toluene, the value given previously in DMSO converts into 39 when the standard potential we have found in the present work is introduced into the thermodynamic cycle. The pK_a of phenol may be estimated as 18.8 in DMF.[21b,d] Figure 9 shows the correlation between the experimental and theoretical ΔpK_as (pK_a(hydrocarbon) − pK_a(phenol)). The theoretical ΔpK_as were obtained from the variation of the electronic energy and of the free energy of solvation (Table 2).[22] The slope of the correlation is significantly larger than 1 for the same reasons as already given in the discussion of the electron-transfer thermodynamics. It is noteworthy that the pK_a of the diphenylmethyl anion exhibits the same anomaly as the standard potential of the diphenylmethyl radical/diphenylmethyl anion couple, although the two quantities derive from independent measurements. The pK_a is larger, and the E^0 more negative, than expected from the comparison with the two other anions because the diphenylmethyl anion is less accessible to solvation and interaction with the countercation.

The driving forces for the protonation of the three anions by phenol are very large, ranging from 12 to 20 in terms of pK_a (Figure 9). Despite this, the protonation rate constants are

(19) (a) Foresman, J. B.; Frisch, A. *Exploring Chemistry with Electronic Structure Methods*; Gaussian Inc.: Pittsburgh, PA, 1996. (b) Foresman, J. B.; Keith, T. A.; Wiberg, K. B. Snoonian, J.; Frisch, M. J. *J. Phys. Chem.* **1996**, *100*, 16098.

(20) Marcus, Y. *Ion Solvation*; Wiley: New York, 1985.

(21) (a) Bordwell, F. G.; Cheng, J.-P.; Harrelson, J. A. *J. Am. Chem. Soc*. **1988**, *110*, 1229. (b) According to pK_a(DMF) = 1.5 + 0.96 pK_a(DMSO). [21c] (c) Maran, F.; Celadon, D.; Severin, M. G.; Vianello, E. *J. Am. Chem. Soc*. **1991**, *113*, 9320. (d) Bordwell, F. G. *Acc. Chem. Res*. **1988**, *21*, 456.

(22) For the phenol−phenate couple, we found $U^0_{el,PhO} - U^0_{el,PhO^-} = -15.62$, $(U^0_{el} + G^0_{solv})_{PhOH} - (U^0_{el} + G^0_{solv})_{PhO^-} = -13.16$, and $G^0_{PhOH} - G^0_{PhO^-} = -12.81$ eV.

Table 3. Half-wave and Standard Potentials

	$E_{1/2}$[a]		
radical	3 μs	1 ms	E^0 [a]
9-anthrylmethyl	−1.035	−1.005	−1.018
diphenylmethyl	−1.115	−1.050	−1.107
benzyl	−1.270	−1.220	−1.215

[a] In volts vs SCE.

clearly below the diffusion limit. If the reaction is under activation control, the values of the rate constant imply large reorganization energies, 2.5, 2.0, and 1.8 eV for the benzyl, diphenylmethyl, and anthrylmethyl anions, respectively, assuming a Marcus-type quadratic activation−driving force relationship. It is noteworthy that the reorganization energy increases as the pK_a increases, unlike what is generally found with carbon acids bearing activating electron-withdrawing groups.[23] One may also envisage, as rate-determining step, the diffusion-controlled formation of a precursor complex in which the anion and the acid would adopt precisely defined relative positions. Further insights into the problem should await the determination of Brönsted plots over a reasonable range of pK_as.

Although the components of the half-wave potential could not be dissected in the case of the 4-methylbenzyl radical, the EPI results indicate that the follow-up deactivation of the anion is faster and the electron transfer slower than with the benzyl radical. Both effects fall in line with the electron-donating properties of the 4-methyl substituent.

Conclusions

Application of the EPI technique has allowed the determination of the reduction mechanism of benzyl, diphenylmethyl, and anthrylmethyl radicals in DMF and the dissection of the half-wave potential into its various components. Besides dimerization of the radical, the reduction is jointly controlled by the kinetics of the electron-transfer step and of a follow-up deactivation of the anion involving acids present or purposely added. The determination of the standard potential and of the rate constants of the electron transfer and follow-up reaction in DMF is made possible by the fact that the latter step is not too fast and the former not too slow. The situation is less favorable in acetonitrile, where the follow-up reaction is faster and the electron transfer slower. There is thus an increased tendency for the reduction to be under the sole kinetic control of the electron-transfer step, as is the case with the benzyl radical. Under such conditions, the half-wave potential represents an irreversible reduction potential from which the contribution of the standard potential and the standard rate constant of electron transfer cannot be separately extracted unless the attending reorganization free energy could be independently estimated. A similar situation is expected in DMF for slower reducing radicals and more reactive anions (4-methylbenzyl radical is one example).

In DMF, the neglect of the kinetic factors in the estimation of the standard potential of the benzyl, diphenylmethyl, and anthrylmethyl radicals, simply equating its value with the value of the half-wave potential, leads to an error which ranges from negligible to ca. 60 mV (1 order of magnitude in terms of equilibrium constants) according to the measurement time (Table 3).

The standard potential of the radicals varies in the order benzyl < diphenylmethyl < anthrylmethyl, as expected intuitively (the π orbital of the radical gets lower and lower in the series). Intuition is confirmed by density functional calculations. Electron transfer to the radicals is relatively fast, but not as fast as it is with aromatic hydrocarbons of similar conjugation. More precisely, reorganization free energies for the electrochemical reaction uncorrected from double-layer effects range from 0.7 to 0.9 eV. Analysis of earlier redox catalysis data and density functional estimations agree and indicate homogeneous self-exchange reorganization free energies ranging from 1.1 to 1.3 eV. Solvent reorganization is amply predominant (the intramolecular reorganization free energy represents about 5% of the total). The relatively large solvent reorganization free energy, as compared to those of anion radicals, is caused by the presence of a large fraction of the negative charge on the benzylic carbon, even if a significant fraction is delocalized over the aromatic ring (more in the case of diphenylmethyl and anthrylmethyl anions that with the benzyl anion, which explains the corresponding increase of the solvent reorganization free energy).

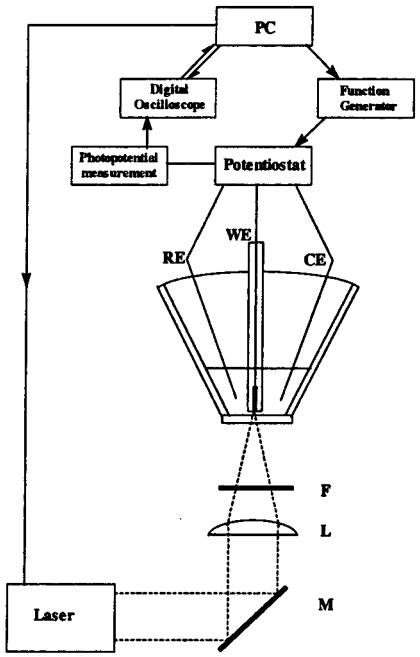

Figure 10. Instrument for the electron photoinjection experiments. WE, RE, CE, working, reference, counter electrodes, respectively; M, semitransparent mirror; L, lens; F, filter.

Protonation of the anions by phenol is highly exergonic (from 12 to 20 pK_a units). It is remarkable that, despite this large driving force, the protonation rate constant is 1.5 orders of magnitude below the diffusion limit. It is also noteworthy that the protonation rate constant does not vary significantly when the driving force varies from 12 to 20 pK_a units.

As compared to the two other anions, diphenylmethyl anion exhibits an anomalous behavior as far as the thermodynamics and kinetics of electron transfer and also its basicity are concerned, which can be explained by some steric hindrance to solvation of its benzylic carbon position.

Experimental Section

Chemicals. The solvents, DMF (Fluka, puriss. 0.01% H_2O) and acetonitrile (Merk-Uvasol) were used as received. Et_4NClO_4 (Fluka, purum), used as supporting electrolyte, was recrystallized from a 1−2 ethyl acetate−ethanol mixture. *n*-Bu_4NPF_6 (Fluka, purum) was recrystallized from a water−ethanol mixture. Phenol and benzyl chloride were purchased from Fluka and diphenylmethyl, 4-methylbenzyl, and 9-anthrylmethyl chlorides from Aldrich. They were used as received.

Instrumentation and Procedures for Electron Photoinjection Experiments. The instrument (Figure 10) includes three elements: an

(23) Bernasconi, C. F. *Adv. Phys. Org. Chem.* **1992**, *27*, 119.

electrochemical cell equipped with three electrodes, a excimer laser delivering a short light pulse onto the working electrode, and an electronic setup which imposes the dc potential of the working electrode and allows the recording and integration of the transient photopotential. The whole system is triggered and controlled by a personal computer.

The working electrode is a 0.5-mm-diameter gold disk, frequently polished with diamond pastes, rinsed with acetone, and ultrasonicated in methylene chloride. The counter electrode is a platinum wire. The reference electrode is an aqueous saturated calomel electrode. Its potential is checked against the ferrocene−ferrocenium couple at the end of each experiment. All potentials given in the text are thus referred the same aqueous SCE. The cell is equipped with a double jacket, allowing it to be thermostated (the temperature was fixed at 20 °C throughout the present study). The bottom of the cell is a quartz window allowing the passage of the light beam, and the tip of the working electrode is positioned 1 mm above the window.

The laser was a Questek 2054 filled with a XeCl mixture (wavelength 308 nm, pulse duration 20−50 μs, pulse stability ±5%). The laser beam is directed toward the cell by semitransparent mirrors and focused onto the surface of the electrode so as to covered a slightly larger area. Filters are used to attenuate the beam when necessary so as to shine an energy of ca. 100 μJ on the electrode surface.

A more detailed sketch of the potentiostat and photopotential measuring device is given in Figure 2 of ref 12b. The sampling resistance R_S was set equal to 100 kΩ in all experiments. The function generator and the digital oscilloscope were Schlumberger 4431 and Tektronix TDS 430A instruments, respectively.

The electrode dc potential is varied incrementally, each 5 mV, so as to cover a potential range of ±200 mV around the half-wave potential. After each of a series of 5−10 laser shots, the photopotential is sampled in the digital oscilloscope at 22 preselected times from 3 μs to 1 ms along a logarithmic incrementation. The resulting photopotential/time curves are averaged, and the averaged curve is transferred to the PC. The same cycle of operations is repeated at each value of the dc potential, and the whole set of data, stored in the PC, is treated so as to display one polarogram for each preselected time.

The substrate concentration was 10−30 mM, with the exception of 9-anthrylmethyl chloride, where a concentration of only 1 mM was used in order to avoid significant absorption of light by the substrate. Even with such a low concentration, the possible generation of the carbanion from the reduction of the radical by solvated electrons remains negligible for the following reasons. Since solvated electrons are potent reductants, the reduction of the radical should proceed at a rate constant close to the diffusion limit, as for their capture by the substrate. As shown elsewhere,[13] the ratio of the average concentrations of carbanions and radicals formed at the end of the capture process is given by the expression $\Gamma^0(k_d/D_e[RX])^{1/2}/\{1 - \exp(-\Gamma^0(k_d/D_e[RX])^{1/2})\} - 1$, where Γ° is the amount of solvated electrons per unit surface area that will be eventually captured (0.9×10^{-13} mol/ cm^2 in the present case), k_d ($= 2 \times 10^{10}$ M s^{-1}) is the diffusion-limited rate constant, and D_e ($=15 \times 10^{-5}$ cm^2 s^{-1}) is the diffusion coefficient of the solvated electrons. It is thus seen that the carbanions formed in this way during the capture process are less than 3% of the radicals formed and have, therefore, no detectable influence on the polarograms and on their variations with time.

Theoretical Modeling. The calculations were performed using the PC-Spartan software 1.1 (Wavefunction Inc., Irvine, CA) and the Gaussian 94[24] package for HF calculations and Gaussian 94 package for density functional and solvation calculations. Gas-phase geometries and electronic energies were calculated by full optimization of the conformations using the B3LYP[25] density functional with the 6-31G* basis set,[26] starting from preliminary optimizations at the HF/6-31G* level. Solvation free energies were calculated on the gas-phase optimized conformations according to the SCRF (self-consistent reaction field) method using the IPCM model[19] and the B3LYP density functional. In this method, the solvent is treated as a continuum of uniform dielectric constant in which the solute is placed into a cavity defined as an isodensity surface of the molecules. The free enthalpies were obtained after appropriate frequency calculations in the case of the benzyl radical and anion.

Supporting Information Available: Drawings of the optimized geometries at the B3LYP/6-31G* level with the corresponding Cartesian coordinates and the distance matrix, followed by the total atomic charges or total spin densities for open-shell calculations in the case of radicals, the values of energies in hartrees, and S**2 showing the spin contamination for the radicals, anions, and hydrocarbons of benzyl, diphenyl, and 9-methylanthryl compounds (24 pages, print/PDF). See any current masthead pages for ordering information and Web access instructions.

JA981801T

(24) Frisch, M. J.; Trucks, G. W.; Schlegel, H. B.; Gill, P. M. W.; Johnson, B. G.; Robb, M. A.; Cheeseman, J. R.; Keith, T.; Petersson, G. A.; Montgomery, J. A.; Raghavachari, K.; Al-Laham, M. A.; Zakrzewski, V. G.; Ortiz, J. V.; Foresman, J. B.; Cioslowski, J.; Stefanov, B. B.; Nanayakkara, A.; Challacombe, M.; Peng, C. Y.; Ayala, P. Y.; Chen, W.; Wong, M. W.; Andres, J. L.; Replogle, E. S.; Gomperts, R.; Martin, R. L.; Fox, D. J.; Binkley, J. S.; Defrees, D. J.; Baker, J.; Stewart, J. P.; Head-Gordon, M.; Gonzalez, C.; Pople, J. A. *Gaussian 94*, Revision E.1; Gaussian, Inc.: Pittsburgh, PA, 1995.

(25) Becke, A. D. *J. Chem. Phys.* **1993**, *98*, 5648.

(26) Hariharan, P. C.; Pople, J. A. *Chem. Phys. Lett*. **1972**, *16*, 217.